Sensing and Bio-Sensing Research 37 (2022) 100512

Contents lists available at ScienceDirect

Sensing and Bio-Sensing Research

journal homepage: www.elsevier.com/locate/sbsr

Advances in Trans-Epithelial Electrical Resistance (TEER) monitoring integration in an Intestinal Barrier-on-Chip (IBoC) platform with microbubbles-tolerant analytical method

Lucia Giampetruzzi [a], Laura Blasi [a,*], Amilcare Barca [b], Elisa Sciurti [a], Tiziano Verri [b], Flavio Casino [a], Pietro Siciliano [a], Luca Francioso [a]

[a] Institute for Microelectronics and Microsystems IMM-CNR, Via per Monteroni "Campus Ecotekne", 73100 Lecce, Italy
[b] Department of Biological and Environmental Sciences and Technologies (DiSTeBA), University of Salento, Via per Monteroni "Campus Ecotekne", 73100 Lecce, Italy

ARTICLE INFO

Keywords:
Organ on chip
Trans-Epithelial Electrical Resistance (TEER)
Transparent biocompatible electrodes
Gut monolayer on a chip
Microbubbles in microfluidics

ABSTRACT

Trans-epithelial resistance (TEER) is one of the most widely performed analysis in vitro methods for monitoring barrier tissue development, formation and functional maturation. It is a basic and important tool for the reproduction of an artificial human epithelium. However, in the design and construction of organ on chip devices, the reliable TEER measurements still remain a challenge, in spite of their efficacy in providing real time information on tissue integrity and function. The observed limitations often concern the nature of the selected electrodes, made with opaque or metal materials that prevent microscopic investigation, their correct and stable reposition that affect the impedance spectroscopy analysis and microbubbles interference. Here, we present a method to perform real time TEER analysis on an Intestinal Barrier-on-Chip (IBoC) using integrated transparent electrodes, by means of impedance spectroscopy analysis and supported by a microbubble-tolerant calculation method. The human Caco-2 cells were used as an in vitro model of the intestinal epithelial cell barrier. Measurements can be carried out even in presence of microbubbles during the analysis, thus allowing application of this analytical method in microfluidic organ on chip devices that must perform *in continuum* for a long time.

1. Introduction

Organ-on-chip (OoC) devices are novel micro-scale in-vitro 2D/3D cell culture platforms employed for mimicking tissue/organ architectures and functionalities. In recent years, OoC technology is widely used to reproduce fundamental tissue barriers, such as the blood-brain barrier, blood retinal barrier, the pulmonary air-liquid interface and the intestinal barrier. A deep understanding of the dynamics and mechanisms of the biological barriers is essential for several studies as valid alternative to conventional in-vitro models [1]. A continuous, non-invasive and reliable 'sensing' of the barrier-forming tissue quality could allow investigation on major aspects of physiological and pathophysiological processes [2,3]. Integrated sensors on OoC platforms have been developed to provide indications on physiological parameters such as temperature, pH, humidity, nutrient content, etc. [4,5]. To obtain meaningful measurements it is often essential to locate the sensor next to the cells, such as pericellular sensors for oxygen and reactive species with short lifetime (e.g. ROS, RNS) [6], or conversely, connected downstream by microfluidics such as those used for glucose/ lactate sensing [7–10].

The Trans-Epithelial Electrical Resistance (TEER) measurement is an important non-invasive method for monitoring the integrity of the epithelial monolayer and the permeability variations due to damage/ disruption of the epithelial cell barrier [11,12]. To date, TEER and permeability tests are challenging assays to perform real-time and high-throughput screening to translate these barriers-on-a-chip into drug, nutrient and xenobiotic discovery [13]. This is in line with several EU-funded projects the EU legislation that encourages the use of OOC technology for in vitro advanced analyses to replace animal testing [14–17].

The current commercially available in vitro devices for TEER measurements, such as trans-well systems, enable to place 'chopstick'-type electrodes on both sides of opposite microfluidic channels in OOC devices [18]. However, the continuous placement/displacement of the electrodes for measuring can easily lead to errors and thus variations of the final resistance (as e.g. differences in resistance related to the length

* Corresponding author.
E-mail address: laura.blasi@cnr.it (L. Blasi).

https://doi.org/10.1016/j.sbsr.2022.100512
Received 23 March 2022; Received in revised form 18 July 2022; Accepted 1 August 2022
Available online 3 August 2022
2214-1804/© 2022 The Authors. Published by Elsevier B.V. This is an open access article under the CC BY-NC-ND license (http://creativecommons.org/licenses/by-nc-nd/4.0/).

of paths through microchannels) [19]. Furthermore, the location of these integrated electrodes limits the investigation on tissue cultures by microscopy/fluorescence analyses, and requires specialized cleanroom processes for fabrication [20,21].

Another crucial problem is the formation of air-bubbles, that are often recurrent in microfluidic long-term cell cultures. They can appear after the fluid filling, or even during experiments due to different factors i.e. the hydrophobic chip fabrication materials (as PDMS, TOPAS®, etc.) or pressure and temperature changes. In literature, several methods are proposed to prevent the bubble formation [22–24].

However, methods identified to eliminate bubbles are not reproducible and depend on the nature and dimension of air bubble [25]. Thus, despite their undesirable and disturbing presence in microfluidic devices, micro/nano-scale bubbles recently start to be considered as an emerging, low cost and efficient tool in microfluidic applications [24,25]. Indeed, many studies have explored their potential use in complex micromanipulations such as cell separation [26] and drug delivery [27].

This paper reports a study on an Intestinal Barrier-on-Chip (IBoC) that contains embedded transparent conductive electrodes to monitor cell growth, together with a dedicated electrical model for bubble-tolerant TEER calculation. The reported method is applicable to other OOC devices with two chambers, thus validating direct TEER detection by using integrated electrodes. Also, this electrodes integration could provide a reusable platform for different sensors, e.g. real-time detection of some relevant ions fluxes across the epithelium and/or other physical parameters [28].

2. Materials and methods

2.1. Configuration of TEER on chip

The proposed IBoC was based on a commercial Topas polymer platform modified with transparent indium tin oxide (ITO) electrodes and a transparent Polyethylene terephthalate (PET) porous membrane (Fig. 1). The membrane is located into a fluidic chamber for supporting the cell culture (23 μm thickness, 0.4 μm pore dimension, $5{\cdot}10^8$ pores cm^{-2} pore density). It separates the cavity into 2 horizontally aligned fluidic chambers to mimic lumen vs. contraluminal (blood) compartments. There is a total of 4 chambers per chip platform. Each chamber has 4 ports two inlets, top and bottom and 2 outlets (top and bottom) to allow for cell culture experiments with the fluidic interface that connects directly the chip to the microfluidic system (Fig. 1A-B). In particular, the Elveflow® pressure & flow control instrument (OB1, MK3) has been used to flow the culture media in/through the chip. It enables to inject different fluid solutions using patented piezoelectric regulators, providing a flow control that is rapid and precise. The controller, reservoirs and chip ports are connected through microfluidic flow sensors that are important to perform efficient control on flux and also by microfluidic tubes through which the culture media flow at a constant rate of 7 μL min^{-1}, while the chips are maintained inside the CO_2 incubator. This permits to collect measurements without chip contamination and/or detrimental cell cultures when moving out the incubator. Fig. 1C shows the custom electrical connection of the electrodes with adapters for flat cables (FFC) to a printed circuit board (PCB) for reliable measurements, easy chip exchange and multiple chip connections. The electrodes were selected for their potential suitability during microscope analysis and histochemical investigations, as the continuous monitoring of cell culture morphology during TEER analysis is a critical evaluation step for comprehensively assessing the experimental effectiveness. The electrodes were patterned on PET substrates with a thickness of 175 μm by wet etching technique. For ITO wet etching a 20% HCl solution in DI water at room temperature has been used; the etching rate was about 15 nm min^{-1}. Transparent Indium Tin Oxide (ITO) electrodes were 200 nm thick and their resistivity is 5.5–6.1 Ohm/square in order to support both for Trans-Epithelial Potential Difference (TEPD) and TEER monitoring during cell culture experiments. In Fig. 1D a chamber was partially filled (pink liquid) with Minimum Essential Eagle Medium (MEM) inserted into apical chamber.

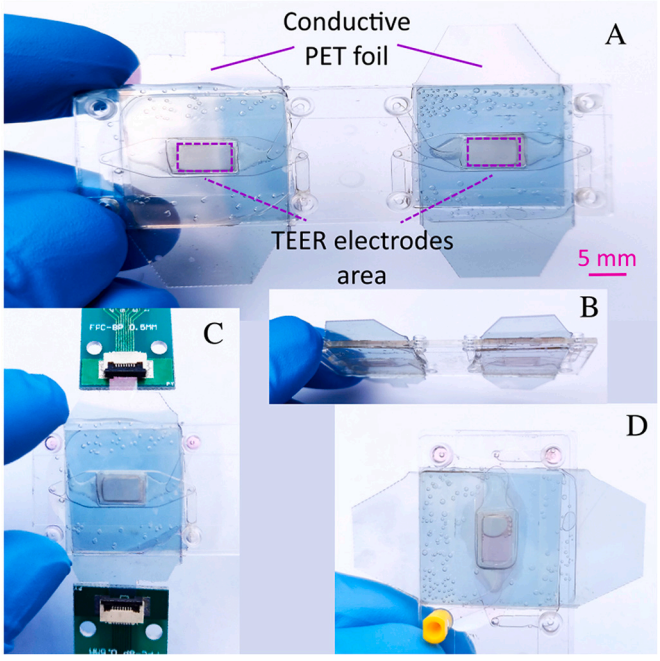


Fig. 1. The details of the modified microfluidic chip: A. Intestinal Barrier-on-Chip with embedded transparent TEER electrodes [dashed borders of cross-sectional measuring area (5×7.3 mm^2)]; B. A detail of top/bottom assembly; C. The custom electrical connection of the electrodes with adapters FFC to a PCB; D. A partially filled chamber with Minimum Essential Eagle Medium (MEM) inserted into the apical chamber.

2.2. Epithelial cell culture conditions and assays

Human intestinal epithelial Caco-2 cells (ATCC® HTB-37™) cells were seeded in the microfluidic device, maintained at 37 °C in a humidified incubator under 5% CO_2 in air and connected to the microfluidic perfusion system. Before cell seeding, the devices were sterilized by UV for 2 h and subsequent washing with a penicillin-streptomycin solution, whereas the circuit system was washed with an ethanol solution. The entire system was then filled with the cell medium. Caco-2 cells were seeded into the upper microchamber at $5{\cdot}10^5$ cells cm^{-2} and allowed to attach under static conditions in complete Minimum Essential Eagle Medium (MEM; Corning). After 4 h, culture medium was perfused through the upper channel at 7 μL min^{-1}. The chips were cultured up to 21 days post seeding to obtain a cells monolayer at the stage of spontaneous enterocyte-like differentiation [29]. The differentiated monolayer was used for TEER analysis and for qualitative fluorescence microscopy assays.

2.2.1. MTT test and cell viability after the integration of transparent conductive electrodes

To assay basic cell-to-chip interactions, e.g. the ability of the chip to support cell viability and proliferation, cell metabolic activity on PET porous membranes and consequent proliferation in the presence of ITO electrodes were investigated by using the 3-(4,5-dimethylthiazol-2-yl)-2,5-diphenyltetrazolium bromide (MTT) assay directly on chip.

2.2.2. Immunofluorescence assay for adherens junctions detection

The presence of a mature monolayer, characterized not only by the appearance of tight junctions (TJ), monitored by TEER, but also by the appearance of other lateral plasma membrane protein structures, such as

adherens junctions (AJ), was evaluated by treating cells with egtazic acid (EGTA) 5 mM dissolved in Dulbecco's calcium chelator phosphate buffered saline, D-PBS, administered for 2, 24 and 48 h. Incubation with EGTA, which is a divalent-cation chelator, decreases calcium levels, thus inhibiting the homo−/hetero-junctions formation by cadherins among adjacent cells. As a consequence of this experimental manoeuvre, protein structures such as TJ proteins disassemble and are internalized [30].

2.3. Impedance spectroscopy and TEER measurements

The TEER electrode system was suited to examine the properties of the functional epithelial monolayer without destroying the device, Impedance spectra were recorded at different time points (0, 3, 7, 10, 14, 21, 24 days) to continuously monitor cell layer formation and maturation in situ. In principle, this approach is based on the impedance spectroscopy technique. Namely, a small amplitude excitation (AC) voltage (10 mV peak-to-peak) with variable frequency is applied to two electrodes located at the top/bottom side of the two chambers, in contact with the cell layer by means of the culture medium. The resulting total impedance, Z, contains information about the TEER and the cell layer capacitance, that can be extracted as parameters, adopting an appropriate equivalent electrical circuit [18].

Several mathematical models and equivalent circuits to derive the impedance of the cellular layer system have been reported in literature [22,31,32]. In Fig. 2 the proposed circuit is different in the equal contribution to the TEER measurements, of the capacitance of electrodes and the R medium at the 2 electrodes located at the top and the bottom of the chip. The 2 electrical resistances areas follow: R_1 and R_2 elements model the culture medium in the upper and lower compartments as an ohmic resistances; 2 constant phase element, CPE1 and CPE2 that describes the frequency dependent behaviour of the medium-electrode interface, C1 the cell apical and basolateral membranes capacitance.

Analysis on impedance spectra were recorded periodically in a range of 24 days using an IVIUM Vertex One potentiostat/impedance analyser (from IVIUM technologies).

In order to conduct TEER measurements with cells cultured in the chip, a similar procedure was repeated for each time point. Generally, before the measurements, the fluid flow was stopped. TEER measurements were carried out, connecting the chip to impedance analyser and keeping 37 °C temperature through an aluminium plate with the PID temperature control in real time. The procedure takes about 2 min for each chamber, for a selected spectrum collection (100 Hz - 10 kHz) over frequencies with most cell-related information and with 5 points for decade. After the TEER measurements the chips were immediately recollected to the flow-system in incubator. The impedance spectra were analysed, with the EIS Spectrum Analyser software.

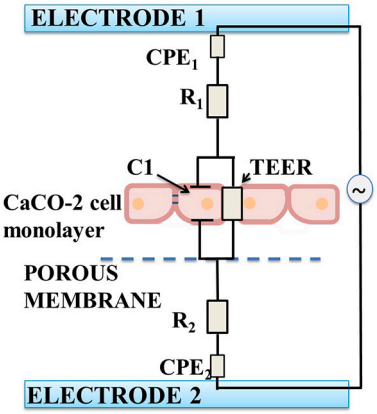


Fig. 2. The proposed equivalent circuit is characterized by the equal contribution to the 2 electrodes of media resistance and the electrodes capacitance. In particular, the cell layer resistance and the cell layer capacitance are in parallel. It is applied and used to analyse the impedance spectrum of CaCo-2 monolayer on chip.

2.4. Development of microbubbles-tolerant algorithm for TEER calculation

Contemporary to the acquisition of impedance spectra, several membrane micrographs at each time point, were acquired by an optical microscope, in order to detect the real area of membranes covered by medium (Fig. 3). Indeed, at the interruption of fluid flow, required to noiseless collect the impedance spectra, it has been noticed that several microbubbles arose in the channels and in the cavities of the cellular membrane. Some microbubbles were also observed by visual inspection in the concave regions of the microchannels (restrictors, channels section variation) in the intermediate days between the measurements, due to chip higher temperature (incubator, 37 °C) with respect to laboratory temperature were the microfluidic controller (and the medium reservoirs) were located (22 °C). Thus, a main innovation of the work was also to demonstrate the validation of a TEER calculation algorithm that is microbubble-tolerant, supplying corrected values for TEER even in case of culture membrane not fully covered by the medium when the measurement is performed. We assume that the measured Z value is actually not related to the entire area of the membranes in chip, but only to effective area without bubbles. The advantage of our approach is related to the assumption that the simple image inspection (and bubble area calculation) can allow a reliable TEER compensation because the microbubbles are trapped between the top/bottom assembly of the cover lid/membrane (by capillary forces), thus breaking the electrical conduction path of the whole bubble footprint within the electrodes.

The presence of air bubbles, between the top cover lid of the chip and the membrane, leads to Z values that are not necessarily increasing. We normalize TEER value using variable areas (according to the area occupied by bubbles, each day of measurement). This approach could enable the in-chip TEER monitoring even when interferences/artefacts emerge into the microfluidic stream for several reasons.

As shown in the diagram of Fig. 4, the effective area without microbubbles has been estimated by the ImageJ ™ software, that highlights the circular spots and calculates the bubble area inside the membrane frame. The resistance obtained by the impedance spectra and the consequent fitting with an equivalent circuit has been normalized on the value of area obtained by the ImageJ™ software, for each membrane analysed and at all selected time points (Fig. 4).

The Fig. 5 reports the rationale of the experiments carried out, with a schematic of our IBoC, with a detail of the suspended PET porous membrane. The microfluidic chip is based on the Fluidic 480 chip (Microfluidic ChipShop, Jena), modified with a custom transparent PET membrane extracted from the same trans-well insert adopted for preliminary Caco-2 seeding experiments and same porosity (see Section 2.1). The image analysis step allows for the microbubble-tolerant TEER algorithm development and consequent standard fluorescence validation of TJ degradation.

3. Results and discussion

3.1. Integration of transparent conductive electrodes, MTT test and cell viability

Before further analyses on actual growth and development of the intestinal cells monolayer, we investigated the cytotoxicity induced by the ITO electrodes inserted into the apical and basolateral compartments and used for TEER measurements. Investigation about potential impact on monolayer viability was assessed by the MTT test, considered as one of the simplest assays used to this scope. The analysis conducted on chip to evaluate cell viability (Fig. 6) showed that the cell layer in the presence of ITO electrodes for 48 and 96 h has the same metabolic activity as the control chips ($p > 0.05$), underling a good biocompatibility of these

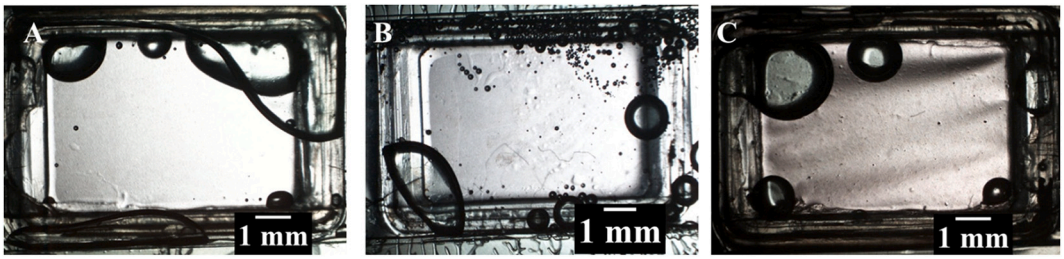


Fig. 3. Microscope images of membranes during TEER measurements at 3 (A), 14 (B), and 24 (C) days post seeding. During the acquisition of the impedance spectra, the fluid flow interruption causes microbubbles that interfere with the resistance estimation.

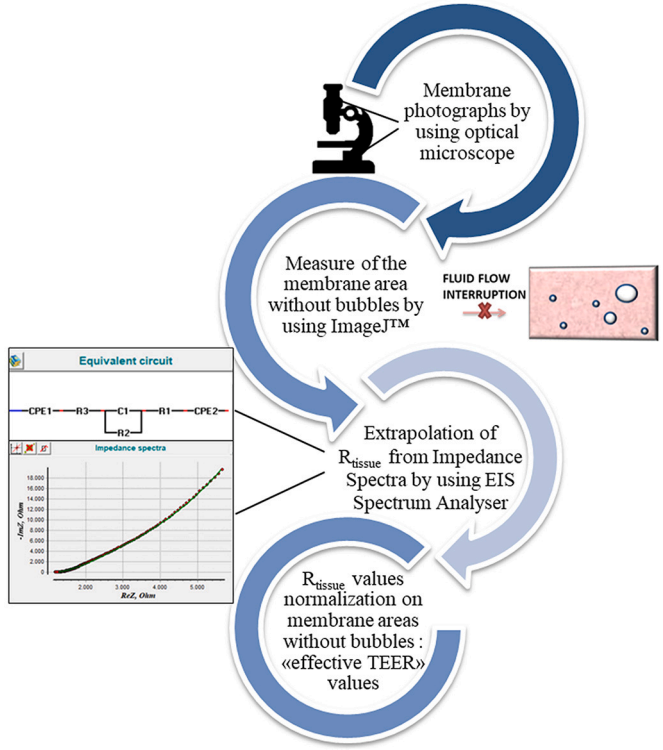


Fig. 4. Flowchart that depicts our microbubbles-tolerant algorithm for TEER calculation. The first step consists in collecting membrane photographs by means of an optical microscope at the selected time points (the same of TEER measurements). From these images it is possible to analyse the membrane areas, and extrapolate the areas without bubbles using ImageJ software ®. Then, after obtaining TEER estimation from impedance spectra by using EIS spectrum analyser, it is possible to calculate the effective TEER value, by multiplying this TEER value with the membrane area without bubbles (at the selected time points).

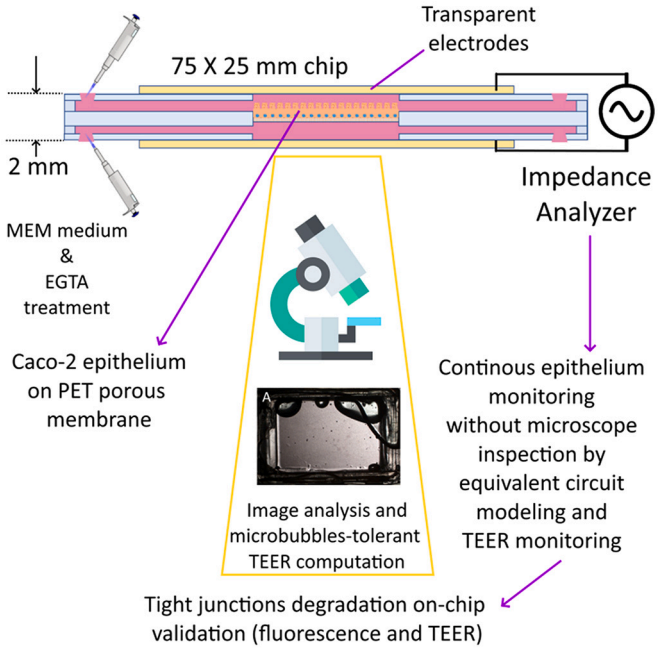


Fig. 5. A schematic picture represents a rationale of the experiments: the custom modified chip for the development of microbubble-tolerant TEER algorithm and for the validation of the standard fluorescence during the monolayer formation and subsequent EGTA triggered tight junctions degradation.

electrodes in contact with the cell medium. The percentage of viability in the 3 samples examined is similar and this data reflects the evaluation recently proposed by other researchers [33].

3.2. Analysis of the impedance spectra and equivalent circuit

Impedance data were analysed for the determination of TEER and cell layer capacitance values of the Caco-2 monolayer's grown on the chip membrane. Some circuit models were adopted from the literature and assessed, considering the fit-reliability and biological criteria described, while the model described in Fig. 2 was adopted to extrapolate features from impedance spectra. In Fig. 7 are shown the typical spectra acquired at different days post seeding (dps) reporting the impedance magnitude (|Z|) vs frequency.

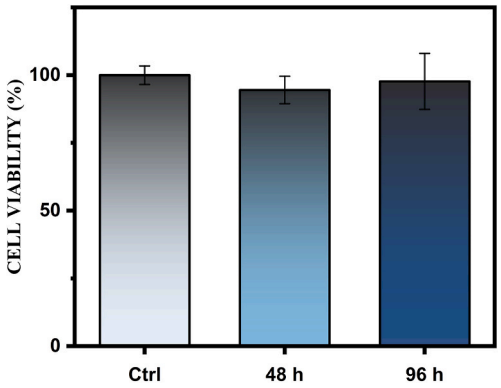


Fig. 6. MTT assay for cell viability with ITO electrodes: histograms represent the percentage (%) with respect to control cells (Ctrl, 100%) of viable cells after the exposure to ITO immersed in MEM medium. Data show means ± SE ($n = 3$). Statistically significant differences with respect to the control according to One-Way ANOVA; $p < 0.05$. Means comparison by Tukey's test.

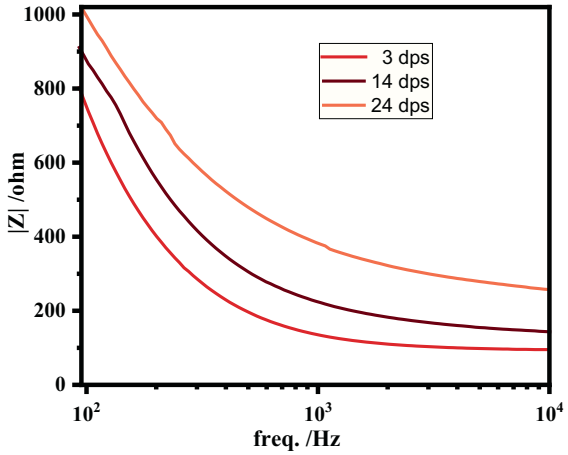


Fig. 7. The typical impedance spectra. The bode plot of impedance magnitude of the Intestinal Barrier-on-Chip at 3, 14 and 24 days post seeding (dps).

Control experiments were carried out by measuring impedance values on empty chambers (for short circuit check) and chambers filled with MEM culture medium. The impedance values corresponding to MEM filled chambers were comparable with those obtained with MEM solution and therefore they were used as background. TEER was then measured in 3 different IBoCs, each containing two chambers, seeded with Caco-2 cells and filled with culture medium in upper and lower compartment. After 24 h, the cells were fed by flowing (7 μL min^{-1}) growth medium through the chambers. All IBoCs were maintained for 24 days in culture, under the same constant flux without any evidence of cell toxicity as shown by the MTT test reported in Fig. 6. TEER measurements were carried out using frequency values ranging from 100 Hz to 10 kHz.

The bode plots of impedance magnitude and phase of the IBoCs are consistent with the continuous growth of the cellular layer towards full confluence, generally obtained around 21 dps. For subsequent data fitting we adopted a circuit made of 6 elements, inspired to the work of Groeber et al. [34] that allows the highest circuital details of the different chip interfaces, the best fitting errors and correlation with real biological function of the circuit elements (Fig. 2). The impedance spectra |Z| confirm the increased impedance value in the mid-range of frequencies (100 Hz - 10 kHz) that mainly accounts for the cell layer TJ formation (impedance modulus increases monotonically).

The trends of the bode plot (Fig. 7) are in good agreement with typical simplified Randles cell, largely adopted for cellular-based devices [35]; in fact the graph shows an impedance decreasing behaviour vs. frequency, reaching impedance plateau values vs. dps for $f > 10^4$ Hz.

These spectra and the subsequent data showed above, are referred to 3 selected time post seeding The first (3dps) is related to the cell attachment to the substrate, 14 dps to a good cell confluence, 24 dps (after 18–21 dps) with the monolayer formation. Here a range between 10^2 and 10^4 Hz is employed as reported in literature [13]; in this range the contribution of the impedance is given only by the cell layer; for values lower than 10^2 Hz the electrodes contribution is predominant, whereas for values $>10^4$ Hz the medium contribution becomes prevalent. The impedance curves were fitted with an equivalent electric model as previously described (Fig. 2). CPE and n were estimated by modelling the experimental data using the equivalent circuit shown in Fig. 2 and the eq. (1) to calculate the capacitance and the TEER of the cell layer.

CPE's impedance is expressed as the reciprocal number of the admittance Y at ω = 1 rad/s with the unit S, as reported in literature [36] and an exponent n equalling 1 or 0 for an ideal capacitor or an ideal resistor, respectively:

$$1/Z = Y = Q_0(j\omega)^n \quad (1)$$

Capacitance rapidly increased for the next 15 days until it reached the value of 144 ± 63 μF; this increment of the TEER value could be associated with the increase of the monolayer surface area. Between days 15 and 24 these values oscillated from 140 to100 μF. A slight reduction of the capacitance value after the 14th day may be explained by the formation of cellular aggregates and small multilayer patches, corresponding to a series of capacitors with lower resulting capacitance value.

The n values of CPEs from the fitting with circuit model remained lower than 1 (0.983 ± 0.023) but upper than 0.5 (0.541 ± 0.036), that can be associated with the formation of mature cells monolayer, more similar to an ideal capacitor than a resistor (Table 1).

TEER measurements were recorded at different days post seeding, and the TEER values were determined for each time point. Calculation of the resistance was performed prior to cell seeding (R_{BLANK}, corresponding to membrane resistance) and after cell seeding (R_{TOT}, membrane + cells). The R_{BLANK} was then subtracted from the R_{TOT} value obtained from the EIS software fitting obtaining the effective R_{TISSUE} value in Ω (as reported, the circuit element related to epithelium resistance)

$$R_{TISSUE} = R_{TOT} - R_{BLANK} \quad (2)$$

The TEER (Ω·cm^2) value is finally determined by normalizing R_{TISSUE} to the effective membrane area, corrected with air bubbles areas. This approach has optimized the extrapolation and interpretation of TEER data, avoiding artefacts derived from microbubbles and/or additional contact resistance that can affect the electrical connections. These TEER values were called "effective TEER" (Fig. 8).

During the first 3 days of cell culture, the TEER values oscillated between an average of 100 Ω·cm^2 (day 1) and 200 Ω·cm^2 (day 3), and then rapidly increased until day 24, according to the progressive establishment of the TJ of the cells growing in monolayer (Fig. 8). The development of a cultured cell layer was monitored by a set of electrical simulations compared with a circuit model with CPEs parameters constant.

The "effective TEER" values are presented as Ω·cm^2 rather than Ω (Fig. 8); since these resistance values are dependent on the surface area of the cultured tissue analysed. An improvement of the cell layer resistance determined TEER increased from 110 Ω·cm^2 (only medium) to about 1000 Ω·cm^2 (cells monolayer), and this result shows good agreement with the data reported in literature It is evident that without the compensation of the raw TEER values by the proposed algorithm, the recorded TEER values showed a not reliable trend, since these values are affected by the microbubbles footprints inside the membrane that induce locally increase/decrease of the current impedance values. The proposed method can be particularly useful in high-throughput devices, since it allows a reliable TEER monitoring even in presence of small bubbles concentred in a part of device, or micro particles, whose detrimental effect on TEER can be compensated by an automatic image

Table 1
The pseudo-capacitance Q of the CPE is expressed per surface area of the electrode and the n value is reported as the CPE's order, important to calculate the capacitance and the TEER of the cell layer.

Time in colture (Dps)	CPE influencing parameters			
	$Q_{CPE1}(S{\cdot}s^n_{CPE1})$	n_{CPE1}	$Q_{CPE2}(S{\cdot}s^n_{CPE2})$	n_{CPE2}
3	1.018E-05 ± 0.55E-06	0.983 ± 0.023	8.722E-05 ± 0.23E-06	0.500 ± 0.069
14	1.973E-05 ± 0.11E-06	1.000 ± 0.258	1.000E-04 ± 0.66 E-05	0.541 ± 0.036
24	1.982E-05 ± 0.94 E-06	1.000 ± 0.034	1.000E-04 ± 2.48 E-05	0.546 ± 0.077

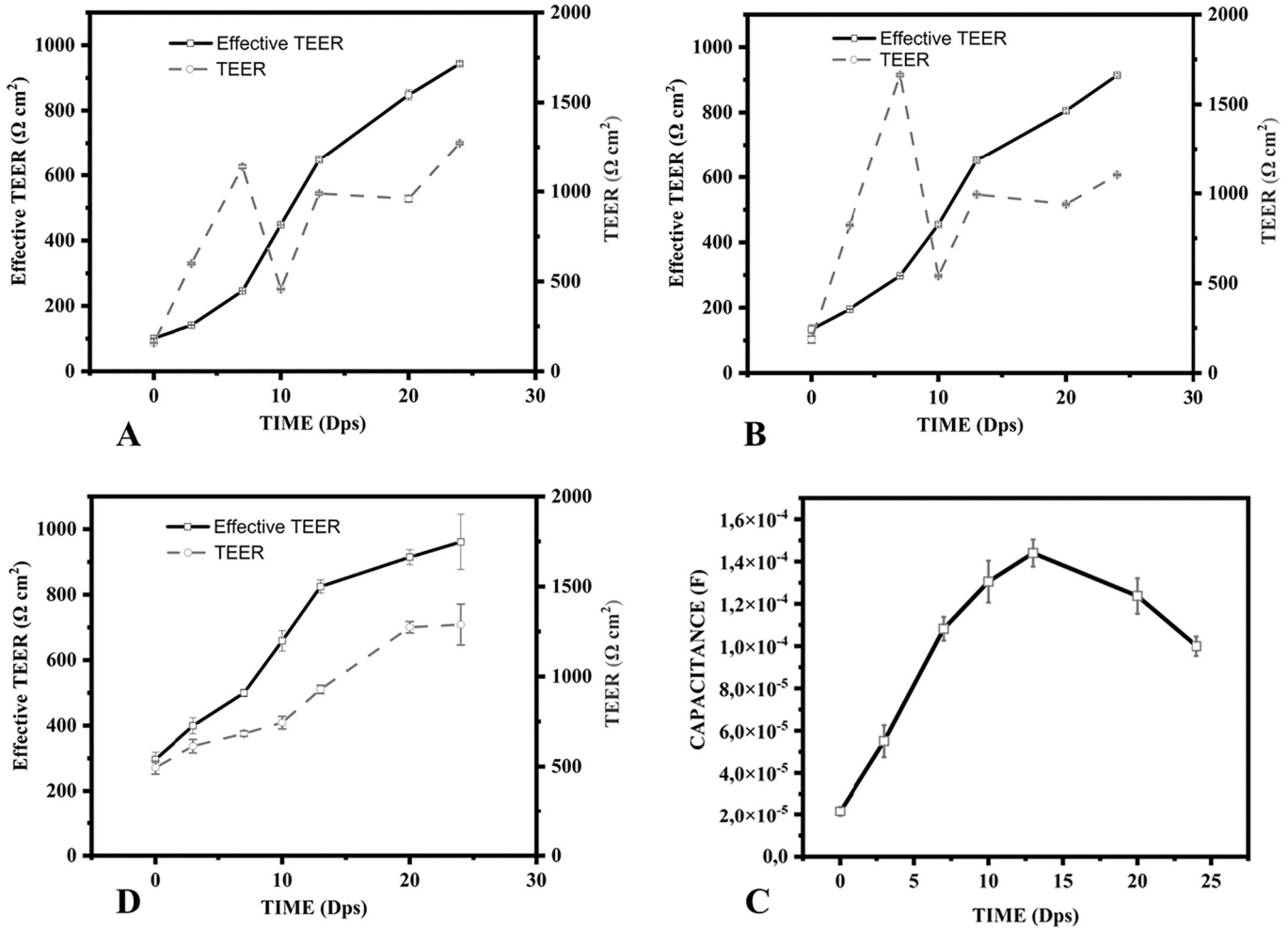


Fig. 8. TEER values (A,B,D), and cellular layer capacitance values (C) until 24 days. The value of effective TEER (normalized on membranes without microbubbles) at 24 days is in line with TEER value of a monolayer of Caco-2 cells growing in conventional 2D techniques.

elaboration. Analysing the capacitance element behaviour, values showed a peak around the 14th day and a slow decrease in the following days (Fig. 8), probably for a suspect cells growth not limited to a monolayer conformation, indeed multiple cells layers with equivalent capacitors in series could induce a total reduced capacitance [37].

Our TEER chip directly measures the impedance of the culture area, without any noises or artefacts due to the repositioning or re-insertion of electrodes. In fact, past TEER studies on trans-well inserts and organs-on-chips normalized their results for total tissue culture area but they were strongly influenced by the electrodes distance from trans-well membrane or by their scarcely repeatable re-positioning at different dps [13].

3.3. Epithelial monolayer formation, EGTA treatment and TEER validation

In present work, the presence of TJ, adherens junction (AJ) and the maturation of the monolayer were also investigated by immunofluorescence assay (Fig. 9). Indeed, cadherin, an AJ protein, is present in the monolayers after 24 days (Fig. 9A) [38]. To experimentally verify that the increase of TEER values measured with our platform was specifically related to the increased growth of TJ, we treated the epithelial monolayer with EGTA in both apical and basolateral compartments at the 24th day.

After the exposure of the epithelial monolayer to EGTA treatment for 2 h and 24 h, TJ and AJ dissociation and disruption are detected, due to the effect of the calcium sequestration by EGTA. This effect was detected by fluorescence imaging (Fig. 9 B, C). Cells lost their adherence on the substrate and the interaction with adjacent cells, thus showing alteration of the epithelial structure, as underlined by restraint of cell morphology, cytoskeletal elements and nucleus [39] [30]. At 48 h the monolayer was completely disrupted and not detectable.

In samples treated with 5 mM EGTA for 2 and 24 h (Fig. 9 B, C), the impedance value related to the bottom side drastically decreased (Fig. 9), because of the destroying of TJ and the increase of permeability.

So, the developed algorithm demonstrates an accurate detection of the monolayer's degradation, keeping separated the TEER contribution of microbubbles (that can hide the TJ and AJ disruption) and the real effect of disruption of barrier features such as integrity.

4. Conclusions

According to the idea that OOC systems need to recapitulate key biological processes and a specific tissue may develop and change with disease, the integration of multiple actuators and sensors in such platforms is crucial to address this ambition [40].

Among the electrically readable properties of epithelia, TEER is a fundamental parameter to assess the proper development of an intestinal tissue. This work proposes a reliable approach for integration of transparent electrodes for TEER monitoring, in conjunction to an algorithmic analysis for monitoring epithelial function even in presence of microbubbles or insulating microparticles.

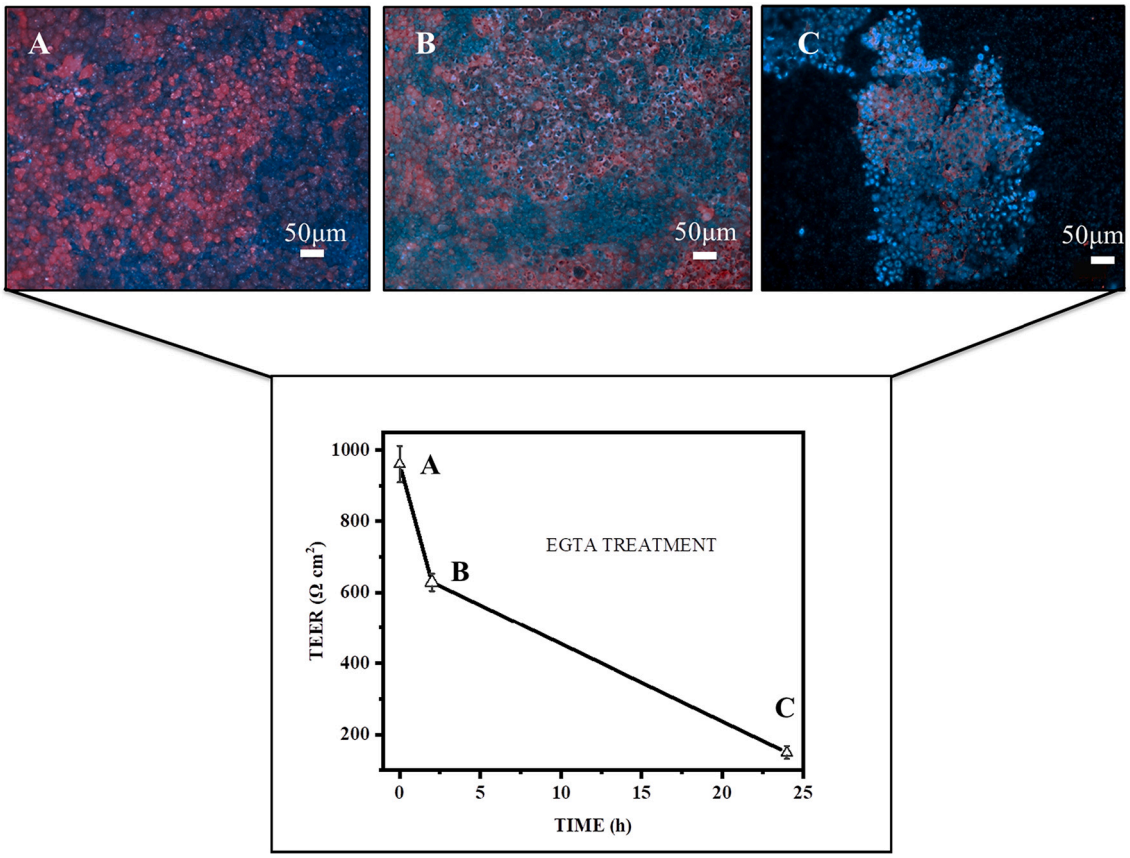


Fig. 9. Microscope micrographs and TEER values about EGTA treatment until 24 h. In A the control sample with the typical epithelial monolayer at 24 days, without treatment. In B the monolayer after 2 h of 5 mM EGTA treatment and in C the monolayer after 24 h of 5 mM EGTA treatment. On the bottom the graph shows the TEER trend after 2 and 24 h of treatment with EGTA 5 mM. The trend is in line with the decrease of tight junctions and the increase of permeability as indicated in the histochemical analysis.

Our microfluidic device can be applied for monitoring the formation of an intestinal epithelium, evidenced by the increase of TEER values during maturation, but also any type of induced injury, as simulated by addition to the culture medium of EGTA (a calcium chelating agent), that has induced an expected abrupt reduction of TEER.

Biocompatibility of all adopted materials is confirmed and high-throughput flat cable connectors for electrical measurements have also been implemented.

The electrochemical analysis has been performed through the impedance spectroscopy method and a consequent fitting with an equivalent circuit for the extrapolation of epithelial TEER and capacitance parameters has been reported. The reported experimental methods on electrodes integration, TEER values compensation and circuital fitting can be applied to commercial microfluidic platform or custom fabricated devices.

The proposed IBoC represents a reliable case study to monitor and determine TEER also in presence of interferences. Our TEER validation method, in the presence of micro- and macro-bubbles, can play a key role in the advancement of recent delivery systems such as ultrasound-driven microbubbles; it is worth to recall that microbubbles have been used as contrast agents in biomedical imaging applied to cancer research [41], thus the translation to intestinal epithelium-on-chip technologies targeted to oncology is actually an intriguing variant of the IBoC application fields.

CRediT authorship contribution statement

Lucia Giampetruzzi: Conceptualization, Methodology, Investigation, Resources, Data curation, Writing – original draft, Visualization. **Laura Blasi:** Investigation, Data curation, Resources. **Amilcare Barca:** Investigation, Visualization, Writing – review & editing. **Elisa Sciurti:** Investigation, Resources. **Tiziano Verri:** Writing – review & editing. **Flavio Casino:** Software, Resources. **Pietro Siciliano:** Supervision, Project administration. **Luca Francioso:** Conceptualization, Methodology, Software, Validation, Supervision.

Declaration of Competing Interest

The authors declare that they have no known competing financial interests or personal relationships that could have appeared to influence the work reported in this paper.

References

[1] M.W. van der Helm, O.Y.F. Henry, A. Bein, T. Hamkins-Indik, M.J. Cronce, W. D. Leineweber, M. Odijk, A.D. van der Meer, L.I. Segerink, D.E. Ingber, Non-invasive sensing of transepithelial barrier function and tissue differentiation in organs-on-chips using impedance spectroscopy, Lab Chip 19 (2019) 452–463, https://doi.org/10.1039/C8LC00129D.

[2] J. König, J. Wells, P.D. Cani, C.L. García-Ródenas, T. Macdonald, A. Mercenier, J. Whyte, F. Troost, R.-J. Brummer, Human Intestinal Barrier Function in Health and Disease 7, 2016, https://doi.org/10.1038/ctg.2016.54.

[3] C.P. Profaci, R.N. Munji, R.S. Pulido, R. Daneman, The blood-brain barrier in health and disease: important unanswered questions, J. Exp. Med. 217 (2020), https://doi.org/10.1084/jem.20190062.

[4] L. Giampetruzzi, A. Barca, F. Casino, S. Capone, T. Verri, P. Siciliano, L. Francioso, Multi-Sensors Integration in a Human Gut-On-Chip Platform, Proc 2, 2018, https://doi.org/10.3390/proceedings2131022.

[5] J. Kieninger, A. Weltin, H. Flamm, G.A. Urban, Microsensor systems for cell metabolism - from 2D culture to organ-on-chip, Lab Chip 18 (2018) 1274–1291, https://doi.org/10.1039/c7lc00942a.

[6] J. Kieninger, K. Aravindalochanan, J.A. Sandvik, E.O. Pettersen, G.A. Urban, Pericellular oxygen monitoring with integrated sensor chips for reproducible cell

culture experiments, Cell Prolif. 47 (2014) 180–188, https://doi.org/10.1111/j.1365-2184.2013.12089.x.
[7] Y. Wu, G. Wu, P. Fu, M. Hu, Microfluidic organ chip for in vitro model of blood glucose monitoring and regulation, E3S Web Conf. 218 (2020) 04029, https://doi.org/10.1051/e3sconf/202021804029.
[8] C. De Pascali, L. Francioso, L. Giampetruzzi, G. Rescio, M.A. Signore, A. Leone, P. Siciliano, Modeling, fabrication and integration of wearable smart sensors in a monitoring platform for diabetic patients, Sensors. 21 (2021), https://doi.org/10.3390/s21051847.
[9] H.H. Nguyen, S.H. Lee, U.J. Lee, C.D. Fermin, M. Kim, Immobilized enzymes in biosensor applications, Materials (Basel) 12 (2019) 121, https://doi.org/10.3390/ma12010121.
[10] A. Weltin, K. Slotwinski, J. Kieninger, I. Moser, G. Jobst, M. Wego, R. Ehret, G. A. Urban, Cell culture monitoring for drug screening and cancer research: a transparent, microfluidic, multi-sensor microsystem, Lab Chip 14 (2014) 138–146, https://doi.org/10.1039/c3lc50759a.
[11] M. Odijk, A.D. van der Meer, D. Levner, H.J. Kim, M.W. van der Helm, L. I. Segerink, J.-P. Frimat, G.A. Hamilton, D.E. Ingber, A. van den Berg, Measuring direct current trans-epithelial electrical resistance in organ-on-a-chip microsystems, Lab Chip 15 (2015) 745–752, https://doi.org/10.1039/C4LC01219D.
[12] P. Zoio, S. Lopes-Ventura, A. Oliva, Barrier-on-a-chip with a modular architecture and integrated sensors for real-time measurement of biological barrier function, Micromachines. 12 (2021), https://doi.org/10.3390/mi12070816.
[13] B. Srinivasan, A.R. Kolli, M.B. Esch, H.E. Abaci, M.L. Shuler, J.J. Hickman, TEER measurement techniques for in vitro barrier model systems, J. Lab. Autom. 20 (2015) 107–126, https://doi.org/10.1177/2211068214561025.
[14] O.J. of the E. Union, Directive 2010/63/EU of the European Parliament and of the Council of 22 September 2010 on the Protection of Animals Used for Scientific Purposes Text With EEA Relevance, Ph. D. Thesis, 2010.
[15] P. UNION, Regulation (EC) no 1223/2009 of the european parliament and of the council, Off. J. Eur. Union L 342 (2009) 59.
[16] E. Commission, Regulation (EC) No 1907/2006 of the European Parliament and of the Council of 18 December 2006 concerning the registration, evaluation, authorisation and restriction of chemicals (REACH), establishing a European Chemicals Agency, amending Directive 1999/4, Off. J. Eur. Union 396 (2006) 1–849.
[17] E. Commission, Regulation (EC) No 1272/2008 of the European Parliament and of the Council of 16 December 2008 on classification, labelling and packaging of substances and mixtures, amending and repealing Directives 67/548/EEC and 1999/45/EC, and amending Regulation (EC), Off. J. Eur. Union 353 (2008) 1–1355.
[18] K. Benson, S. Cramer, H.-J. Galla, Impedance-based cell monitoring: barrier properties and beyond, Fluids Barriers CNS 10 (2013) 5, https://doi.org/10.1186/2045-8118-10-5.
[19] E.G.B.M. Bossink, M. Zakharova, D.S. de Bruijn, M. Odijk, L.I. Segerink, Measuring barrier function in organ-on-chips with cleanroom-free integration of multiplexable electrodes, Lab Chip 21 (2021) 2040–2049, https://doi.org/10.1039/d0lc01289k.
[20] M.W.A.U.- van der Helm, M.A.U.- Odijk, J.-P.A.U.- Frimat, A.D.A.U.- van der Meer, J.C.T.A.U.- Eijkel, A.A.U.- van den Berg, L.I. AU-Segerink, Fabrication and validation of an organ-on-chip system with integrated electrodes to directly quantify transendothelial electrical resistance, JoVE. (2017) e56334, https://doi.org/10.3791/56334.
[21] S.M. Bonk, M. Stubbe, S.M. Buehler, C. Tautorat, W. Baumann, E.-D. Klinkenberg, J. Gimsa, Design and characterization of a sensorized microfluidic cell-culture system with electro-thermal micro-pumps and sensors for cell adhesion, oxygen, and pH on a glass chip, Biosens. 5 (2015), https://doi.org/10.3390/bios5030513.
[22] Y. Wang, D. Lee, L. Zhang, H. Jeon, J.E. Mendoza-Elias, T.A. Harvat, S.Z. Hassan, A. Zhou, D.T. Eddington, J. Oberholzer, Systematic prevention of bubble formation and accumulation for long-term culture of pancreatic islet cells in microfluidic device, Biomed. Microdevices 14 (2012) 419–426, https://doi.org/10.1007/s10544-011-9618-3.
[23] S. Richert, O. Peters, V.H. Nguyen, U. Schnakenberg, Design Concepts for Preventing Gas Bubble Interference in Microfluidic Devices, 2016.
[24] J.H. Sung, M.L. Shuler, Prevention of air bubble formation in a microfluidic perfusion cell culture system using a microscale bubble trap, Biomed. Microdevices 11 (2009) 731–738.
[25] Y. Gao, M. Wu, Y. Lin, J. Xu, Trapping and control of bubbles in various microfluidic applications, Lab Chip 20 (2020) 4512–4527, https://doi.org/10.1039/d0lc00906g.
[26] N. Garg, T.M. Westerhof, V. Liu, R. Liu, E.L. Nelson, A.P. Lee, Whole-blood sorting, enrichment and in situ immunolabeling of cellular subsets using acoustic microstreaming, Microsyst. Nanoeng. 4 (2018) 17085, https://doi.org/10.1038/micronano.2017.85.
[27] K. Kooiman, H.J. Vos, M. Versluis, N. de Jong, Acoustic behavior of microbubbles and implications for drug delivery, Adv. Drug Deliv. Rev. 72 (2014) 28–48, https://doi.org/10.1016/j.addr.2014.03.003.
[28] L. Giampetruzzi, A. Barca, C. De Pascali, S. Capone, T. Verri, P. Siciliano, F. Casino, L. Francioso, in: B. Andò, F. Baldini, C. Di Natale, V. Ferrari, V. Marletta, G. Marrazza, V. Militello, G. Miolo, M. Rossi, L. Scalise, P. Siciliano (Eds.), Human Organ-on-a-Chip: Around the Intestine Bends BT - Sensors, Springer International Publishing, Cham, 2019, pp. 181–188.
[29] I.J. Hidalgo, T.J. Raub, R.T. Borchardt, Characterization of the human colon carcinoma cell line (Caco-2) as a model system for intestinal epithelial permeability, Gastroenterology. 96 (1989) 736–749, https://doi.org/10.1016/S0016-5085(89)80072-1.
[30] S. Tria, L.H. Jimison, A. Hama, M. Bongo, R.M. Owens, Sensing of EGTA mediated barrier tissue disruption with an organic transistor, Biosensors. 3 (2013) 44–57, https://doi.org/10.3390/bios3010044.
[31] J.P. Vigh, A. Kincses, B. Ozgür, F.R. Walter, A.R. Santa-Maria, S. Valkai, M. Vastag, W. Neuhaus, B. Brodin, A. Dér, M.A. Deli, Transendothelial electrical resistance measurement across the blood–brain barrier: a critical review of methods, Micromachines. 12 (2021), https://doi.org/10.3390/mi12060685.
[32] J.G. DeStefano, J.J. Jamieson, R.M. Linville, P.C. Searson, Benchmarking in vitro tissue-engineered blood–brain barrier models, Fluids Barriers CNS 15 (2018) 32, https://doi.org/10.1186/s12987-018-0117-2.
[33] S.-H. Moon, Y.-W. Cho, H.-E. Shim, J.-H. Choi, C.-H. Jung, I.-T. Hwang, S.-W. Kang, Electrically stimulable indium tin oxide plate for long-term in vitro cardiomyocyte culture, Biomater. Res. 24 (2020) 10, https://doi.org/10.1186/s40824-020-00189-0.
[34] F. Groeber, L. Engelhardt, S. Egger, H. Werthmann, M. Monaghan, H. Walles, J. Hansmann, Impedance spectroscopy for the non-destructive evaluation of in vitro epidermal models, Pharm. Res. 32 (2015) 1845–1854.
[35] J.E.B. Randles, Kinetics of rapid electrode reactions, Discuss. Faraday Soc. 1 (1947) 11–19.
[36] O.Y.F. Henry, R. Villenave, M.J. Cronce, W.D. Leineweber, M.A. Benz, D.E. Ingber, Organs-on-chips with integrated electrodes for trans-epithelial electrical resistance (TEER) measurements of human epithelial barrier function, Lab Chip 17 (2017) 2264–2271, https://doi.org/10.1039/c7lc00155j.
[37] T. Gerasimenko, S. Nikulin, G. Zakharova, A. Poloznikov, V. Petrov, A. Baranova, A. Tonevitsky, Impedance spectroscopy as a tool for monitoring performance in 3D models of epithelial tissues, Front. Bioeng. Biotechnol. 7 (2020), https://doi.org/10.3389/fbioe.2019.00474.
[38] W. Meng, M. Takeichi, Adherens junction: molecular architecture and regulation, Cold Spring Harb. Perspect. Biol. 1 (2009), a002899, https://doi.org/10.1101/cshperspect.a002899.
[39] M.A. Garcia, W.J. Nelson, N. Chavez, Cell–cell junctions organize structural and signaling networks, Cold Spring Harb. Perspect. Biol. 10 (2018), a029181.
[40] E. Ferrari, C. Palma, S. Vesentini, P. Occhetta, M. Rasponi, Integrating biosensors in organs-on-chip devices: a perspective on current strategies to monitor microphysiological systems, Biosensors. 10 (2020) 110.
[41] M.J.K. Blomley, J.C. Cooke, E.C. Unger, M.J. Monaghan, D.O. Cosgrove, Microbubble contrast agents: a new era in ultrasound, Bmj. 322 (2001) 1222–1225.